

CMOS-based avalanche photodiodes for direct particle detection

Christopher J. Stapels^{*,a}, Michael R. Squillante^a, William G. Lawrence^a, Frank L. Augustine^b,
and James F. Christian^a

^aRadiation Monitoring Devices 44 Hunt Street, Watertown, MA 02054, USA

^bAugustine Engineering, 2115 Park Dale Ln, Encinitas, MA USA

Elsevier use only: Received date here; revised date here; accepted date here

Abstract

Active Pixel Sensors (APSs) in CMOS (complementary metal-oxide-semiconductor) technology are augmenting Charge-Coupled Devices (CCDs) as imaging devices and cameras in some demanding optical imaging applications. Radiation Monitoring Devices is investigating the APS concept for nuclear detection applications and has successfully migrated avalanche-photodiode pixel fabrication to a CMOS environment, creating pixel detectors that can be operated with internal gain as proportional detectors. Amplification of the signal within the diode allows identification of events previously hidden within the readout noise of the electronics. Such devices can be used to read out a scintillation crystal, as in SPECT or PET, and as direct-conversion particle detectors. The charge produced by an ionizing particle in the epitaxial layer is collected by an electric field within the diode in each pixel. The monolithic integration of the readout circuitry with the pixel sensors represents an improved design compared to the current hybrid-detector technology that requires wire or bump bonding. In this work, we investigate designs for CMOS avalanche photodiode (APD) detector elements and compare these to typical values for large area devices. We characterize the achievable detector gain and the gain uniformity over the active area. The excess noise in two different pixel structures is compared. The CMOS APD performance is demonstrated by measuring the energy spectra of x-rays from ⁵⁵Fe.

© 2001 Elsevier Science. All rights reserved

Avalanche photodiode, APD, particle detector, vertex, APS

1. Introduction

CMOS APS imaging devices provide a low-cost alternative to CCDs, however, the readout noise in the CMOS devices frequently limits their performance. Fabricating CMOS APS devices with pixels capable of amplifying the signal allows the identification of events previously hidden within the readout noise of the electronics. The internal gain of APD devices enables the amplification signals at the pixel.

Avalanche photodiode pixels have been successfully fabricated in commercially available CMOS processes. The diodes have diameters from 5 microns up to 150 microns. When bias is applied to the device, charge pairs generated in the pixel are accelerated by the electric field and multiplied by impact ionization, increasing the

signal amplitude. We have recorded pulse height gains of over 1000 from light-emitting-diode (LED) signals. Figure 1 shows a cartoon of the multiplication process in the CMOS APD pixel.

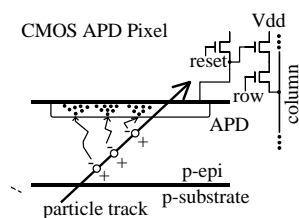


Figure 1. Charge generation from an incident high-energy particle.

When operated below the reverse-bias breakdown voltage, the CMOS APD pixels produce an output signal that is proportional to the input signal while providing internal gain. We refer to this traditional APD operating mode as

* Corresponding author. Tel.: 617-668-6896; fax: 617-668-6891; e-mail: CStapels@RMDInc.com.

“proportional mode”. Uses of diodes operated in this mode include direct particle detection, as in high-energy physics experiments. The extremely small size of the pixels allows high precision position determination.

2. Experimental

Quantum efficiency as a function of wavelength is measured against a calibrated photodiode (Hamamatsu S1336-8BQ) using incandescent light filtered through a monochromator. We measure the quantum efficiency (QE) profile by scanning a focused 632-nm HeNe laser across the surface of the device. A picoammeter measures the photocurrent as the position of the laser focus is scanned. The proportional mode gain is measured by illuminating the pixel with a pulsed, 470-nm LED. Unity gain is assumed when the diode is biased below 5 V. The pulse width driving the LED is adjusted until the maximum signal derived from the leading edge is achieved ($\sim 4 \mu\text{s}$).

A 5.9-keV x-ray provides a reference for the pulse height amplitude. Due to the extremely small size of these detector elements, a very strong ^{55}Fe x-ray source is required to cause an appreciable count rate. Our source is 10 mCi, and spread out over a 6-mm-diameter disc. At the typical distance of 3 mm, approximately 1820 x-rays pass through the 60-micron-diameter pixels per second. At high APD gains, the 5.9-keV x-ray source provides an energy calibration since the average number of electron-hole pairs created in the photoelectric event in silicon is a known value of 1640. The detector output is fed into a Canberra 2004 preamplifier and then a Canberra 2021 spectroscopy amplifier, where the gain is adjusted so that the output signal is in the range of 0 to 5 V, and the shaping time is $0.25 \mu\text{s}$. An Amptek multi-channel analyzer (MCA) records the amplifier output, and the peak centroids are determined using the Origin software package’s Gaussian fit routine.

The multiplication process in the APD introduces noise, which is quantified by the excess noise factor. The excess noise factor is manifest in the width of an external light source compared to a tail pulse generator coupled to the preamplifier input through a capacitor. The tail pulse peak includes the noise associated with the readout electronics and from the dark current in the detector. The ^{55}Fe signal provides a corroborating reference at high gain settings, but is not visible above the noise at low gain settings. For unity gain spectra, the theoretical position of the x-ray peak was adjusted until the excess noise factor was unity. We compute the excess noise factor using the method described in [1]. The excess noise factor is calculated from:

$$F = \frac{(W_L^2 - W_P^2)}{\varepsilon \cdot E_L \cdot 2.35^2}, \quad (1)$$

where E_L and W_L are the centroid and FWHM of the LED signal in units of eV and W_P is the width of a tail pulse signal AC coupled into the preamplifier test input. The value ε is 3.6 eV per electron-hole pair, and the 2.35^2 converts the FWHM values into rms.

3. Results

3.1. Characterization of CMOS APD Pixels

To characterize the proportional-mode performance of the device, we measure the QE for detecting optical photons, at unity gain, as a function of the wavelength. Figure 2 compares the quantum efficiency of two different pixel designs, labeled as “Design 4” and “Design 12”.

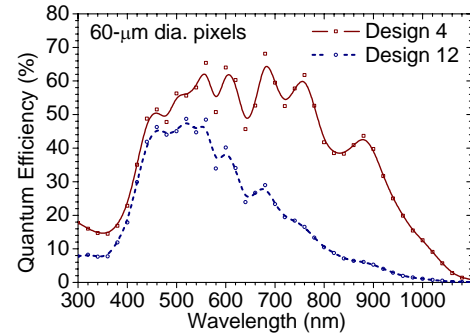


Figure 2. Plot of Quantum Efficiency (QE) as a function of wavelength for two different pixel designs, denoted as “Pixel Design 4” and “Pixel Design 12”. The variations at the peak are due to interference effects from a surface layer.

The p-on-n design, type 12, isolates the avalanche junction from the substrate, resulting in a shallower device that loses QE at long wavelengths ($>700 \text{ nm}$). Figure 3 provides a cross-sectional illustration of these diode designs.

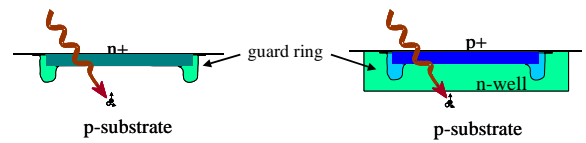


Figure 3. Structure of the pixel designated as “design 4” (left), an “n-on-p”, common anode structure and structure of the pixel designated “design 12” (right), a “p-on-n” structure that is isolated from the substrate.

In the design-4 pixel, we expect that charge pairs generated in the p-substrate below the junction will migrate to the junction where they undergo avalanche multiplication. The design-12 pixel has an isolated n-well, and we do not expect charges generated below this region to be transported to the avalanche junction. This infers that a minimum ionizing particle (MIP) will produce a larger signal in the design-4 pixel, compared to the design-12 pixel, because it collects all of the charges in the ~ 15 -micron thick epi-layer; unlike the design-12 pixel, which will collect charge in the n-well at the top of the epi-layer.

In addition to measuring the quantum efficiency and gain of the CMOS APD pixel, we perform profile scans across the pixel to measure the uniformity and reflectance of the pixel and surrounding structures. Figure 4 plots the response of a 30- μm -diameter design-12 pixel to CW light and the intensity of the reflected signal, superimposed over a photograph on the pixel.

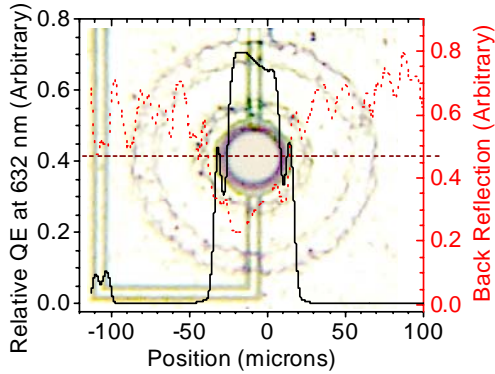


Figure 4. Pulsed 632-nm laser scan of the surface of a 30-micron diameter pixel. The dashed line across the figure shows the path of the focused laser. The left axis plots the relative QE, while the right axis references intensity of the back reflected light, which is the dashed red curve.

The profile in Figure 4 demonstrates a relatively uniform QE within the pixel, and that the reflection of the light from the surface of the pixel is primarily responsible for the QE variations. An aluminum over-layer covers the regions of the chip outside of the pixel, and the reflection measurements show that this layer has a rough surface. The figure also shows signals in the pixel when the focused laser scans over a break in the aluminum layer.

When illuminated under gain, some smaller pixels display some “fringe” effects where the gain near the edges of the pixel is substantially smaller than the maximum gain over a reasonable large proportion of the pixel. To investigate this effect, we scanned the surface of a 150- μm -diameter design-12 pixel at unity gain and at a gain of 2, plotted in Figure 5.

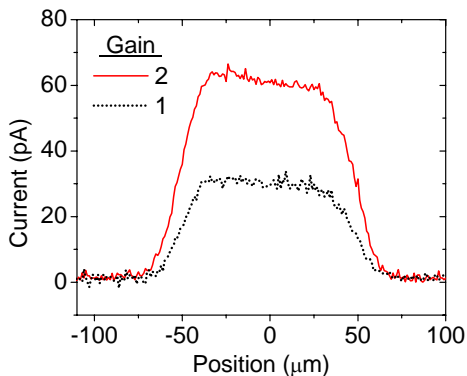


Figure 5. Pulsed 632-nm-laser scan of the surface of 150-micron diameter pixel at unity gain and at a gain of 2. The unity gain is uniform within 5%.

In this case, the fringe effects were minimal and the variation in gain over the active area of the pixel is less than 5%.

3.2. Studies with ^{55}Fe

The primary function of vertex tracking detectors used in high-energy physics experiments is to provide position information that can allow reconstruction of the originating event. Information on the amount of energy deposited in the detector can also be helpful. The low energy 5.9-keV x-ray from ^{55}Fe mimics the magnitude of charge left by a high-energy particle passing through the detector. It provides a useful basis for calibration since the primary absorption mechanism of the x-ray is the photoelectric effect. Figure 6 shows a spectrum of 5.9-keV photons on a 30-micron-diameter pixel.

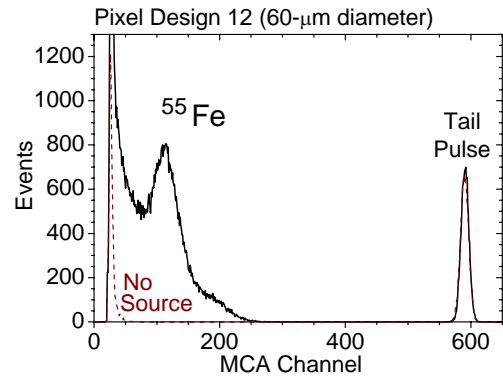


Figure 6. Spectrum of ^{55}Fe x-ray photons incident on a 60-micron diameter pixel at a gain of ~ 30 .

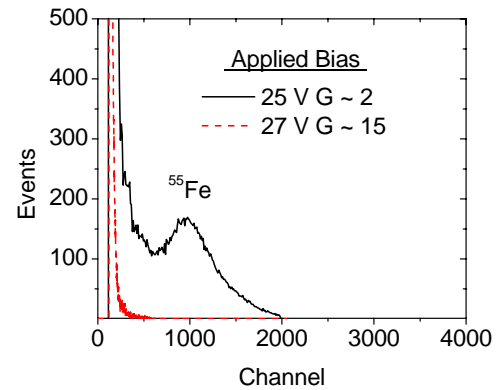


Figure 7. X-ray spectra for two different bias values in pixel design 12, illustrating the ability of the internal gain in the CMOS APD pixel to extract the iron signal hidden in the noise.

Extremely high-energy particles, known as MIPs (Minimum Ionizing Particles) deposit approximately 80 electron-hole pairs per micron. For the design-4 pixel, the epitaxial layer of 10 microns allows for 800 charge pairs. At a gain of only 10, the 8000-electron signal can be discriminated from the noise. Indeed, Figure 7 shows the extraction of ^{55}Fe signals from the readout noise when the applied bias is changed.

3.3. Excess noise factor

The use of internal gain to amplify signals above the noise is constrained by the excess noise, or gain noise associated with the multiplication process. Figure 8 shows a series of excess noise measurements taken for two different size detectors of two different designs at several values of the gain.

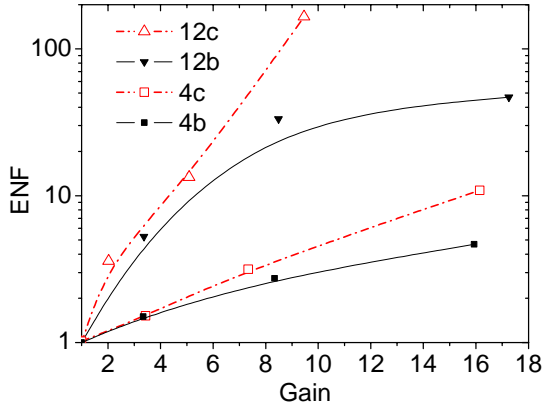


Figure 8. Excess noise factor for four pixels of different designs and size. The designation “c” refers to a 60- μm -diameter pixel, while the “b” refers to a 30- μm -diameter pixel.

The design-12 pixel has a consistently higher excess noise factor. The effect is thought to be due to the difference in the initiator of the event, as described by Zappa, *et al.* [2]. In the design-12 pixel, the incident 470-nm light creates a charge pair in the n-well, and the hole is carried across the junction. In the design-4 pixel, hole pairs are generated in the p-substrate and electrons are multiplied at the junction, resulting in a substantially lower excess noise. Although the design-4 pixel demonstrated generally lower excess noise, the design-12 pixel was able to achieve a higher uniform gain for low energy x-rays.

3.4. Comparison with large area avalanche diodes

These CMOS devices share potential applications with large area APD devices such as those commercially available from, for example, Hamamatsu and Radiation Monitoring Devices. Farrell *et al.* [3, 4] have published some standard comparisons of the large area devices. The large area devices generally have a correspondingly large depletion width and are operated at a much higher bias (1-2 kV). The hole-to-electron ionization probability, or k , is much closer to unity in these large area devices, so that the excess noise factor generally stays near 2 for the better commercially available devices.

The table below summarizes some of our characterizations. The bulk and surface current are determined from a fit to the dark current at several different gains.

Table 1. Characterization of CMOS avalanche photodiodes to standard commercial LAAPD's. I_{dc} is the total dark current, while I_{ds} and I_{db} are the surface and bulk components, determined by examining the I-V curve.

	LAAPD	CMOS APD 4c
Active Area	170 mm ²	0.028 mm ² per pixel
QE	>70	>60
Capacitance	110 pF	1.8 pF (est.)
Gain (M)	<1000	<150
F	2.2 (M=200)	3 (M=10)
I_{dc}	~2000 nA	2.6 pA
I_{ds}	~400 nA	2.6 pA
I_{db}	~8 nA	~0.03 pA
$\sigma_{p/amp}$, [e]	~11.5	12
σ_{ds} , [e]	1.8	1.7
σ_{db} , [e]	60	120
σ_{noise} , [e]	8	120

The excess noise factors are generally higher than standard linear-mode large area APDs. The abruptness of the junction doping is thought to lead to a large k value. Although the noise factor in our devices is generally higher than commercially available devices at a similar gain, the internal gain at the pixel level enables the detection of signals that would otherwise be buried in noise fluctuations.

- [1] M. Moszynski., "Large area avalanche photodiodes in scintillation and X-rays detection," *Nuc. Inst. & Meth. in Phys. Res A*, vol. 485, pp. 504-521, 2002.
- [2] F. Zappa, A. L. Lacaita, and C. Samori, "Impact of local-negative-feedback on the MRS avalanche photodetector operation," *IEEE Trans. Electron Devices (USA)*, vol. 45, pp. 91-7, 1998.
- [3] K. S. Shah, R. Farrell, R. F. Grazioso, L. Cirignano, M. R. Squillante, and G. Entine, "Planar processed APDs and APD arrays for scintillation detection," presented at 1999 IEEE Nuclear Science Symposium. Conference Record. 1999 Nuclear Science Symposium and Medical Imaging Conference (Cat. No.99CH37019), 1999.
- [4] P. Shagin, P. Cushman, K. S. Shah, R. Farrell, M. McClish, and L. Cirignano, "Multipixel APD Photodetector for Charged Particle Tracker," presented at IEEE NSS, Rome, Italy, 2004.